Asian Pub. Corp.

www.asianpubs.org

ARTICLE

Identification of Novel Anticancer Agent by *in silico* Methods for Inhibition of KLK-12 Protein

Jyothi Bandi[1] and Navaneetha Nambigari[1,2,✉]

Asian Journal of Organic & Medicinal Chemistry

Volume: 6 Year: 2021
Issue: 1 Month: January–March
pp: 13–23
DOI: https://doi.org/10.14233/ajomc.2021.AJOMC-P304

Received: 21 December 2020
Accepted: 30 January 2021
Published: 24 March 2021

ABSTRACT

A critical route for cancer metastases is pathological angiogenesis. The protein Kallikrein-12 (KLK-12) is a serine protease reported to be involved in a variety of biochemical processes that have a functional role in angiogenesis. The KLK-12 protein hydrolyzes the cysteine rich angiogenic inducer 61 (CYR61) protein and controls the bioavailability of angiogenesis-inducing growth factors. The work proposed involves the homology modeling of the KLK-12 protein, identify essential residues to be putatively linked to the natural substrate. Protein-protein docking is done to characterize Trp35, Gln36, Gly38, Trp82 and His107 residues of the active site, in addition to active site servers (active site prediction server and CASTp). Using Auto Dock Vina software, virtual screening studies were carried out to identify the substituted carboxamide scaffolds as a pharmacophore binding at the active site. Based on binding energy, ADME and visual inspection, an isochromene carboxamide moiety is identified as antiangiogenic and cancer antagonists.

KEYWORDS

Kallikrein, Angiogenesis, Homology, Virtual screening, Pharmacophore.

INTRODUCTION

Cancer is a life-threatening condition that is characterized by uncontrolled growth and spread of tumour cells. Tumor growth and metastases are dependent on angiogenesis, the growth of new blood vessels from pre-existing blood vessels [1,2]. The process involves the development and release of angiogenic growth factors such as vascular endothelial growth factor (VEGF), fibroblast growth factor-2 (FGF-2) and transforming growth factor-β (TGFβ), which bind to endothelial cell receptors. Endothelial receptor binding and activation lead to endothelial cell proliferation and migration, resulting in tumor expansion exponentially [3,4]. Therefore, angiogenesis is a critical phase in tumor development, invasion and metastases. Recent studies have shown that the angiogenesis deregulation plays a central role in the pathogenesis of many diseases including cancer, several ocular disorders, various skin diseases and impaired wound healing [5].

Kallikrein proteins are mysteriously expressed in several forms of cancer [6]. The kallikrein gene and protein symbols are shown as KLK [7,8]. Human tissue kallikreins (KLKs) promote angiogenesis directly by disrupting the extra cellular matrix (ECM) barriers or indirectly by activating multiple matrix

Author affiliations:

[1]Department of Chemistry, University College of Science, Osmania University, Tarnaka, Hyderabad-500007, India
[2]Department of Chemistry, University College of Science, Saifabad, Osmania University, Hyderabad-500004, India

✉To whom correspondence to be addressed:

E-mail: navaneeta@osmania.ac.in; nitha379@gmail.com

Available online at: http://ajomc.asianpubs.org

metalloproteinases (MMPs) through the urokinase plasminogen activator/UPA receptor (uPA/UPAR) activation pathway [9]. Human tissue kallikreins (KLKs) consist of 15 homologous trypsin or chemotrypsin-like serine proteases. KLK proteins are pre-proenzymes containing an amino-terminal signal sequence (Pre), a propeptide (Pro) that preserves them as inactive precursors (zymogens) and the serine-protease domain responsible for catalytic activity [10]. KLK-12 is a recently discovered kallikrein expressed in breast cancer tissues [11].

Studies show that the Kallikrein like peptidase-12 (KLK-12) is a trypsin-like serine protease that promotes angiogenesis through the cleavage of ECM-associated signaling proteins in the CCN family. Fig. 1 demonstrates the mediation of KLK-12 *via* the cleavage of ECM protein, Cysteine-rich angiogenic inducer 61 (CYR61) to release intact VEGF, FGF-2 and TGFβ from its complex to induce angiogenesis [6,12]. Proteolysis of CYR61 by KLK-12 protein contributes to the release and activation of VEGF, TGFβ & FGF-2. Activation of these growth factors contributes to tumor angiogenesis. Impediment of KLK-12 activity with specific anti-KLK-12 antibodies has been reported to reduce the spread, migration and development of microvascular endothelial cell branching cords *in vitro* [13,14]. The proposed work deals with the identification of new small inhibitor molecules of pathogenic angiogenesis by considering KLK-12 protein as a novel target.

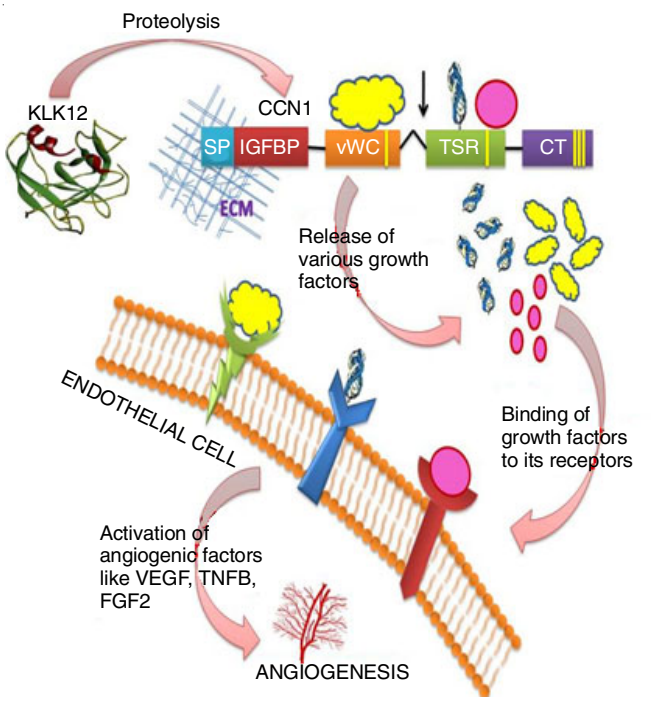

Fig. 1. Biochemical Pathway of KLK-12 protein. SP: Secretory signal peptide, IGFBP: IGF-Binding protein domain, vWC: von Willebrand type C domain, TSP: Thrombospondin domain, CT: Cysteine Knot domain, Plasma membrane, Fibroblast growth factor2 (FGF-2), vascular endothelial growth factor (VEGF), extracellular membrane, target protein KLK-12, transforming growth factor β (TGF β), TGFβ receptor, VEGF receptor, FGF receptor, Integrin binding site, Cleavage site CCN1 by KLK-12

Bioinformatics tools deliver a new area of personalized medicine aimed at more reliable and effective diagnosis and treatment of human diseases. This will operate in a short period of time and can suggest the correct prescription for the right patient at the right time, which will greatly increase the quality of treatment and reduce healthcare costs [15]. This area of medicine needs precise molecular knowledge on the pathology of DNA, RNA and protein levels of human diseases [16]. Bio-profiles such as proteomics, genomics and metabolomics, along with other bioinformatics techniques, may be a promising potential method for the healthcare system [17].

EXPERIMENTAL

Homology modeling: Homology modeling is a very significant computational method used to determine the 3D structure of proteins, in the absence of PDB either by X-ray crystallography, or NMR spectroscopy or electron microscopy. Comparative homology modeling is a multistep process [18]. The present study involves (i) homology modeling, (ii) evaluation and refinement of predicted 3D structure, (iii) active site identification and (iv) virtual screening and ADME prediction [19-22].

The fasta sequence of KLK-12 protein (177 amino acids) is retrieved [23] from UniProt [24] of Expert Protein Analysis System (ExPASy) Server [25,26] with Uniprot ID E9PR22. A protein sequence (Template) similar to KLK-12 protein sequence is identified using NCBI-BLASTp [27] JPred [28], HHPred [29] servers based on the parameters of sequence similarity, secondary structure, and fold recognition. The template protein is considered based on the criteria of the score and E-value obtained [30]. Pairwise alignment of the KLK-12 protein sequence with the template is carried out using Clustal W [31]. The 3D structure of KLK-12 protein is built using the MODELLER 9v9 program [32]. Among the generated 200 models, the model with the lowest modeller objective function is selected for further refinement.

Evaluation and refinement of 3D structure KLK-12 protein: The generated 3D model of KLK-12 protein is refined by loop building using Swiss PDB viewer (SPDBV 4.10) [33], which computes bad contacts using the conjugate gradient method. The 3D model is subjected to energy minimization by adding hydrogens. The refined and energy minimized model is validated by the PROCHECK server to measure the geometry of all amino acids of the protein using Psi and Phi torsion angles [34]. The stereochemical quality of the 3D protein is elucidated with Ramachandran Plot. ProSA server is used to predict the overall fold and local model quality [35]. The stable conformation of the KLK-12 protein has been evaluated for its specific structural features and credible active site regions.

Active site identification and protein-protein docking: Identifying the active site region is an important step in the design of drugs. Computed atlas of protein surface topography, CASTp [36] server, active site prediction server tools and literature are used to predict the active site regions in the KLK-12 protein. These server tools measure the area and volume of each cavity to assess the active site domain. The protein-protein docking is performed by employing a Fast Fourier transformation method using the Patch Dock server program [37,38]. The KLK-12 protein is docked with its natural substrate CYR61 (PDB ID: 4D0Z-A). The docked complex of KLK-12-CYR61 is evaluated to confirm the putative binding interactions.

Virtual screening: The energy minimized 3D protein structure is considered for virtual screening to identify the new lead molecules. Virtual screening studies were attempted to explore the binding mode of the suggested inhibitors onto the 3D model of KLK-12 using AUTODOCK tools 1.5.6 (ADT) [39]. Ligand centered maps were generated by AutoGrid program with a spacing of 0.375 Å and grid dimensions of 44 × 58 × 44 $Å^3$. Grid box center was set to coordinate-27.285, -4.168 and -8.415 in *x*, *y* and *z*, respectively. All water molecules were removed and ADT software was used to prepare the required files for AutoDockVina by assigning hydrogen polarities, calculating Gasteiger charges calculation using AUTODOCK tools available from Scripps Research Institute (http://www.scripps.edu/mb/olson/doc/Autodock) and converting protein structures from the .PDB file format to .PDBQT format [40,41]. Diverse library containing 99, 288 diverse drug-like molecules were used for screening. RMSD values are calculated for the lowest energy pose and the experimental coordinates. The RMSD value below 3.0 Å is considered to be acceptable [42,43]. The predicted binding energies of three best-scored poses of the top-ranked compounds among the compounds screened and physico-chemical properties of ligands can also be retrieved and also performed Swiss ADME [44].

ADME: The new Swiss ADME web tool is used to adapt fast but robust predictive models for physico-chemical properties, pharmacokinetics, drug-likeness and drug-chemistry-friendliness, including in-house proficient methods such as BOILEDEgg, iLOGP and Bioavailability Radar [45]. The rationale for drug molecules to fail in drug development is undesirable absorption, delivery, metabolic processing.

As a consequence, the production of drugs is becoming a difficult task. Additional literature on ligand molecules' ADME properties takes us down a fascinating track with valuable knowledge for the development of effective molecules for drugs. To predict the drug-able properties of ligand molecules, computational ADME properties can be calculated. To conclude, it gives an idea of compound selection for drug discovery. New hits were listed as KLK-12 binding energy-dependent protein inhibitors, RMSD, visual inspection and prediction of ADME, KLK-12 new hit protein screening was performed.

RESULTS AND DISCUSSION

The present study treats KLK-12 as a novel target for the detection of new leads as a drug candidate for pathogenic angiogenesis inhibition. Bioinformatics methods are used to test the 3D structure of the target protein. Virtual screening experiments were conducted against the active site of KLK-12 for the discovery of novel lead molecules. The fasta sequence of KLK-12 protein (target) with a length of 177 amino acids was retrieved from the Expasy server and template searched by different servers (NCBI-Blast, JPred and HHpred). Position-specific iterative simple local alignment search tool (PSI-BLAST) [46] module used to identify the homologous amino acid sequence of protein KLK-12 as a template. The stochastic model used in the BLAST programme describes a prototype with the closest identity to the target [47]. The low E-value of 1NPM-A is of high relevance in terms of the biological relationship to the amino acid sequence of KLK-12.

The Jpred4 server identified template proteins with homologous secondary structure prediction, solvent accessibility and coil-coil region prediction by applying multiple sequence alignment profiles. Jpred4 uses the JNet algorithm [48], which allows the identification of the most probable secondary structural elements (α-helices, β-sheets and loops) in the proteins which are deposited in the PDB. The secondary structure proposed by the Jpred4 server tool matches the KLK family prototype, namely 1NPM-A.

HHpred server uses the statistical framework of the information in the insert and eliminates the probabilities. The server uses pair-wise query-template alignment or multiple query alignment templates selected from the search results, as well as 3D structural models determined from these alignments by the MODELLER program. HHpred allows a pair wise profile comparisons of hidden Markov models (HMMs) [49]. Based on the HMM – HMM comparison and E – value = 2e – 25, the estimated template structure is 1NPM-A.

Table-1 reflects the E-Score of various template search servers on the basis of which Neuropsin with PDB ID: 1NPM-A is selected as a template protein. Based on the results obtained from NCBI-BLASTp, JPred4, and HHpred data analysis, 1NPM – A (retrieved from the RSC protein data bank) was verified as a valid template for KLK-12 protein sequence modelling. The pair wise alignment of the KLK-12 protein sequence with the protein template sequence was performed using ClustalW (Fig. 2). The KLK-12 protein sequence is therefore believed to be specifically consistent with the phylogenetic sequence of proteins, which is a prerequisite for the design of a valid and practical 3D structure.

TABLE-1
TEMPLATE SELECTION FOR KLK-12 PROTEIN

Server	Parameter(s)	E-value	PDB code
BLAST	Sequence specificity	2e-35	1NPM-A
JPred 4	Secondary structure	8e-29	1NPM-A
HHPred	Sequence, secondary structure	2e-25	1NPM-A

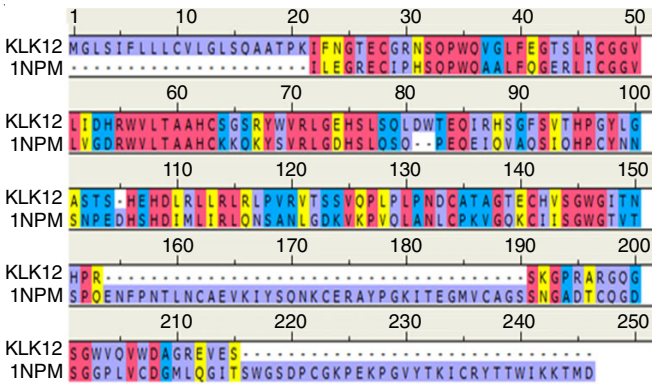

Fig. 2. Alignment of KLK-12 with template protein. Pair wise sequence alignment of the KLK-12 sequence and its template was performed with CLUSTAL W and analyzed in Discovery Studios 3.5. The figure shows preserved amino acid residues (Red), strongly similar (Black), weakly similar (Blue) and a grey colour for diversity

MODELLER 9v9 was used to create a 3D model of KLK-12 protein structure. At first, 200 models were built and the model with the lowest Modeller objective function was selected for further refinement. The developed 3D model is further

optimized by loop modeling and energy minimization using the Swiss PDB Viewer 4.1.0 [50]. Local minima-7.493.9 × 10^{-3} kcal/mol of energy for the refined KLK-12 model was observed.

The accuracy of the model can be further enhanced by confining the structure to a web-based molecular dynamic analysis in locPREFMD (local protein structure refining *via* molecular dynamics) [51]. Table-2 displays the molecular dynamics (MD) simulation refined data for KLK-12 and the overall factors are optimized after the simulations. The results show that the stability parameters of the KLK-12 structure improved significantly following the application of the molecular dynamics. The conformational change observed in terms of the RMSD value, before and after minimization in the initial and final KLK-12 models is 0.77 Å.

TABLE-2
MOLECULAR DYNAMIC DIMENSIONS OF THE STABILIZED STRUCTURE OF KLK-12

Parameter checked	Initial value	Refined value	Goal
phi-psi backbone favoured region	81.400	94.100	> 90
phi-psi backbone allowed region	15.900	-0.14	<-1
phi-psi backbone general region	2.800	0.700	<-2
phi-psi backbone unflavoured region	0.091	0.057	< 0.2%
chi1-chi2 side chain disallowed region	0.078	0.056	< 0.2%
G-factor covalent bonds	0.150	0.050	> -0.5
G-factor overall interactions	-0.280	-0.290	> -0.5
Favourable main chain bond lengths	100.000	100.000	100%
Favourable main chain angles	94.600	92.700	100%
Side chain ring planarity	68.900	93.400	100%

The architecture of KLK-12 protein after energy minimization was further stabilized by performing a molecular dynamics experiment in the locPREFMD serve. The obtained values show that KLK-12 dynamically stabilized model has by far the most stable conformation. The RMSD of the 3D protein after refining *via* MD simulation is 0.77 Å, which is considered to be stable and reliable (RMSD < 2.0 Å) for further studies. The 3D model inferred by homology modeling is shown in Fig. 3 has 8 β strands and 2 helices, which is consistent with its family of KLK family proteins.

The results of the NCBI-BLASTp server show that target KLK-12 protein sequence has a trypsin-like serine protease (Tryp_SPc) domain from amino acid 22 to 150 as shown in Fig. 4. This Tryp_SPc domain is involved in proteolysis of CYR61 by KLK-12 proteins and is present in the N-terminal region of KLK-12.

The stereochemical quality of 3D structure of KLK-12 was validated by the Ramachandran contour map (Fig. 5). Psi and Phi angles for the refined 3D structure of the protein KLK-12 were defined using PROCHECK. The preferred region is in red, the additionally permitted region is in yellow, the generously allowed region is in light yellow and the disallowed region is in white. The Ramachandran plot statistical analysis shows that 98.6% and 1.4% of the residues are in the most energetically preferred and additionally enabled region; and none of the residues contained in the disallowed region show that the

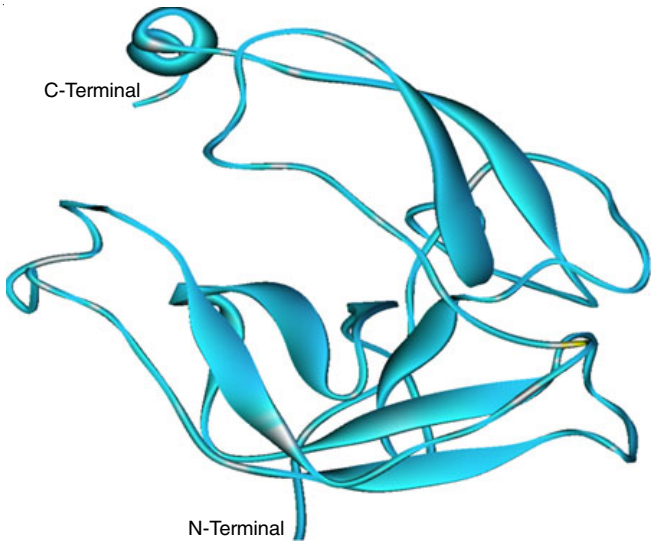

Fig. 3. 3D Structure of KLK-12 protein showing secondary structure

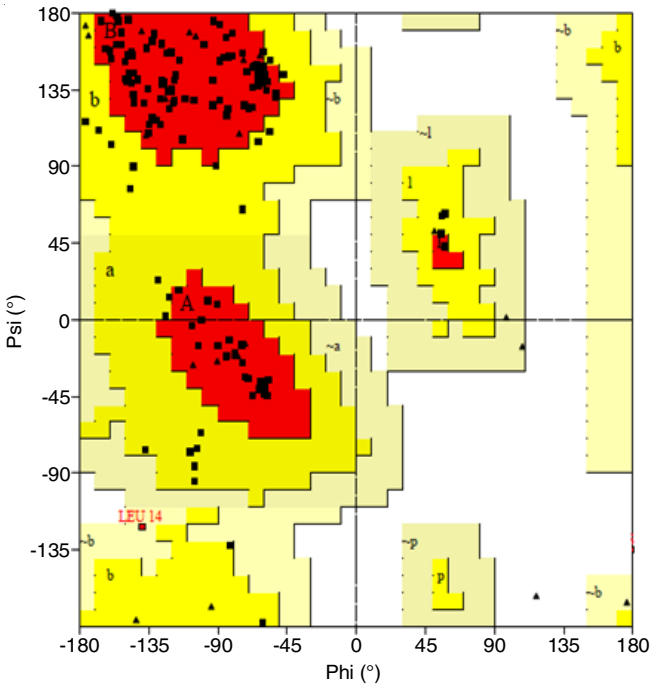

Fig. 5. Stereochemical quality of the KLK-12 protein

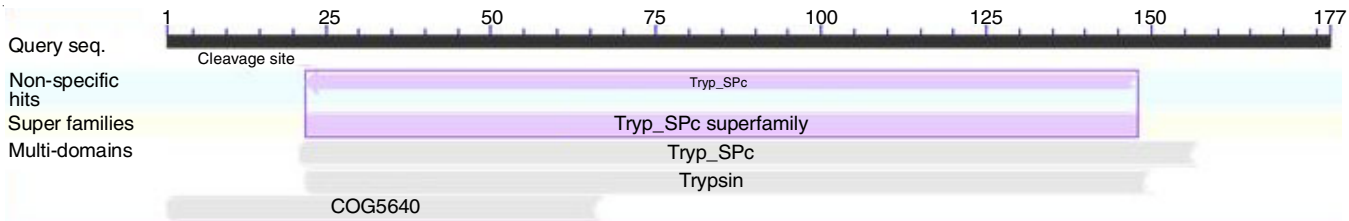

Fig. 4. Conserved domain of the KLK-12 protein. The pictorial representation of the local similarity search result obtained by BLAST

expected 3D model of KLK-12 protein is a good quality model. The plot of Ramachandran shows a total of 98.6% of KLK-12 residues in the most preferred region is considered as a good indicator for further studies.

The overall quality of KLK-12 model was further assessed by the ProSA server (Fig. 6A), the server measures the ProSA II plot based on the folding protein energy of the amino acid sequence. The ProSA web server confirms the overall and local model accuracy of the target protein by comparing it with the protein structure of a similar amino acid length stored in the PDB. Fig. 6A shows that the overall folding energy of KLK-12 protein is negative with a Z-score of -2.44 (seen as dark spot in the dark blue region) suggesting that the target protein 3D model is very close to the experimentally determined NMR structures. This value shows the high overall quality of the KLK-12 protein model.

ProSA's energy profile (Fig. 6B) provides protein-energy in two segments (window size 10 and window size 40 amino acids) and tests the accuracy of the local protein model using knowledge-based energy values. The low-energy profile that defines the local KLK-12 model output as reliable.

The 3D model of KLK-12 protein is submitted for secondary structure analysis to the PDB sum server. It has 2 α-helices, 8 β-sheets and 5 β-hairpins. The amino acid spectrum of helix H1 is from Trp56 to Thr59 and helix H2 from Trp169 to Ser177 (Fig. 7). The eight (8) β-sheets are from Gly29-Trp35, Glu41-Cys47, Leu51-Arg55, Ser64-Trp69, Leu80-Phe91, His107-Leu114, Thr138-Trp145, Arg159-Val168.The five (5) β-hairpin loops are Gln36-Phe50, Gly48-Val50, Val70-Gln79, Ser92-Glu106, Gly146-Ala158 (Fig. 7). The kallikrein family of proteins such as KLK 5, KLK 7 also contains the same secondary structure from amino acid 29 to amino acid 180. The

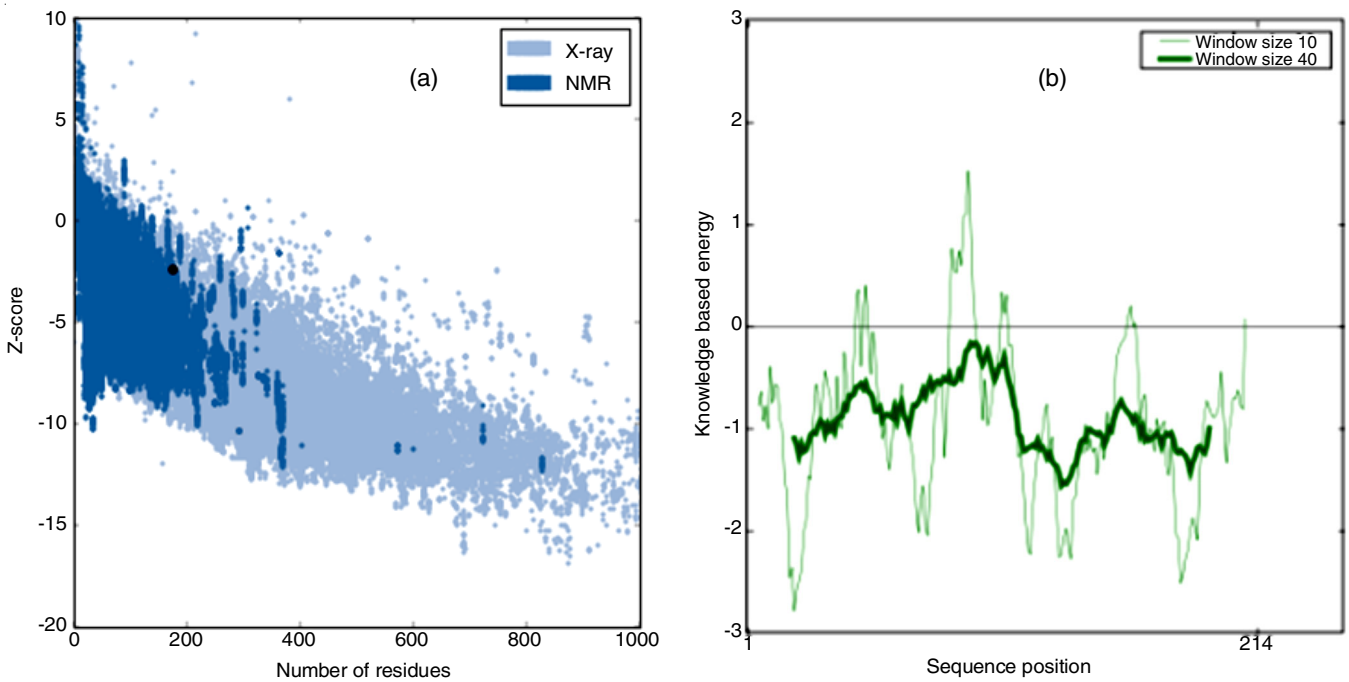

Fig. 6. Overall and local quality of the KLK-12 protein. (a) The Z-score (Black dot) calculated from the ProSA server for KLK-12 proteinis-2.44. The ProSA plot depicted X-ray crystallography (light blue) and NMR spectroscopy(dark blue) for all proteins in PDB. (b) Knowledge-based energy profile of amino acids with a window size of 10 amino acids (light green) and a window size of 40 amino acids (dark green)

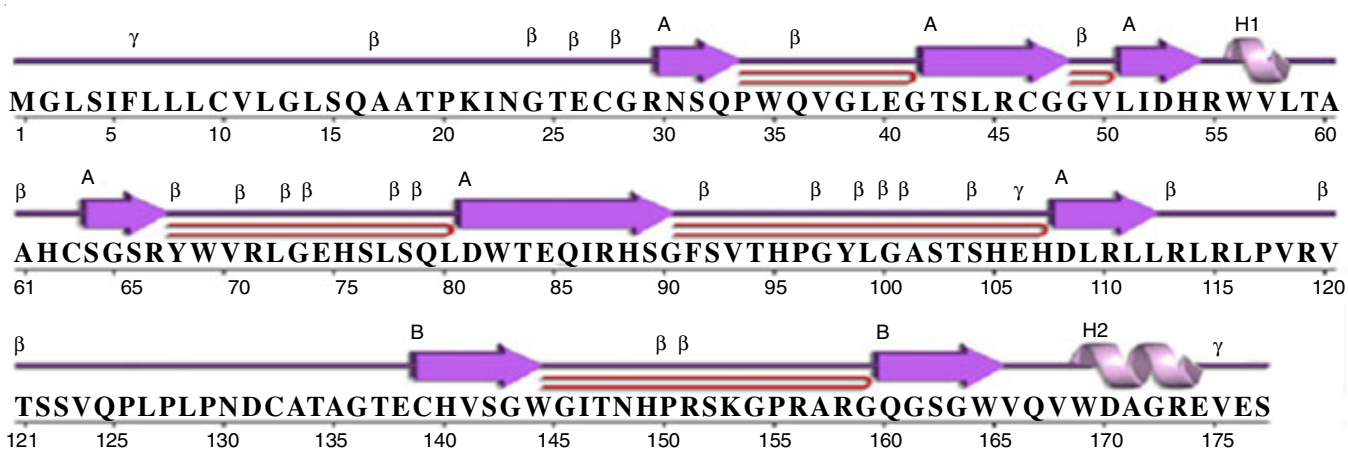

Fig. 7. Secondary structure elements of KLK-12 protein as obtained from PDB sum server

KLK-12 protein secondary structure shows 2α helices and 8β sheets.

Further study of the secondary structure of KLK-12 protein model shows the presence of three salt bridges Glu27-Arg 30 (2.939 Å), Arg 55-Glu 106, (3.073 & 3.401 Å), which give extra stability to the structure. It can be inferred from the anal-ysis of the secondary structure that the homology model produced is reliable.

The interactions study in the protein-protein complex KLK-12-CYR 61 offers a comprehensive overview of the putative binding region in KLK-12, which is essential for activation responsible for angiogenesis. The KLK-12 binding pockets involved in interaction with its natural cascade signaling receptor are identified from the CASTp server and the active site predi-ction server. The results of the servers on analysis display two binding pockets as shown in Table-3. Both servers identified the presence of two pockets in the same conserved area. The wide hydrophobic region of CASTp server covers the conserved domain of amino acids 30 to 58 and amino acids 91 to 150 of KLK-12 protein. The small hydrophobic region covers the N-terminal β-hairpin and β sheets which range from amino acid 32 to 50.

TABLE-3
AMINO ACID RESIDUES IN THE BINDING POCKETS OF KLK-12 PROTEIN

Pocket No.	Volume (Å)^3	Amino acid residues	Number of amino acids in the pocket
		CASTp	
1	4525.7	GLN, GLY, ASP, CYS, SER, VAL, LEU, ASN, HIS, PRO, THR, GLU	59
2	475.3	GLY, PRO, ARG, TRP, GLU, SER, GLN	21
		Active site prediction server	
1	1475	THR, SER, HIS, GLU, ASP, LEU, ASN, PRO, CYS, THR, ALA, GLU, VAL	51
2	1310	GLY, SER, THR, HIS, ASP, LEU, PRO, ARG, TRP, GLU, GLY, GLN	39

Amino acid residues in the binding pockets of KLK-12 protein as obtained from CASTp and active site prediction servers with its volume.

In addition to the identification of amino acid residues involved in the binding, the protein-protein interaction (PPI) studies were performed between KLK-12 and CYR 61 using the Patch Dock server. The input used for docking is the CYR 61 receptor protein recovered from the protein data bank (PDB ID: 4D0Z-A) at a resolution of 2.1 Å and the 3D model of KLK-12. The receptor was prepared by eliminating all hetero-atom's, including water and by adding polar hydrogen atoms. Both the receptor and KLK-12 PDB files have been uploaded. The RMSD was set to 4 Å the rest of the parameters being set to the default settings. The results of Patch Dock were obtained as a series of scoring functions based on the complementarity of shape and the atomic de-solvation energy of the transformed complex. The docked complex of KLK-12-CYR61 proteins has 16 hydrogen bond interactions (Table-4). The amino acid residues identified that are important for binding are Pro20, Lys21, Gln36, Gly38, Ser78, Asp81, Arg115, Arg119 and Arg157, which are also present in the conserved KLK-12 protein domain as shown in Fig. 8.

TABLE-4
HYDROGEN BOND INTERACTIONS OF KLK-12 AND CYR61

S. No.	Amino acid residues KLK-12 and CYR61	Distance (Å)
1	GLN36:O---A:ALA268:HN	1.7
2	GLY38:H---A:ASP269:OD2	1.3
3	PRO20:O---A:TYR471:HH	2.1
4	LYS21:H---A:TYR471:OH	2.0
5	LYS21:HZ3---A:CYS473:O	2.2
6	SER78:HG---A:MET258:SD	2.4
7	SER78:O---A:ASN257:HD21	2.4
8	ARG119:HE---A:ASP259:OD2	2.4
9	ARG119:HH11---A:ASP259:OD1	2.1
10	ARG119:HH21---A:TYR99:OH	2.1
11	ARG119:HH21---A:ASP259:OD1	1.3
12	ARG119:HH22---A:ASP259:OD2	2.2
13	ARG115:O---A:GLN262:HE22	1.8
14	ASP81:OD1---A:ASN257:HD21	2.4
15	ARG157:HE---A:TYR284:OH	2.3
16	ARG157:HH12---A: ALA476: O	2.3

*Amino acid residues represented as 3 letter codes.

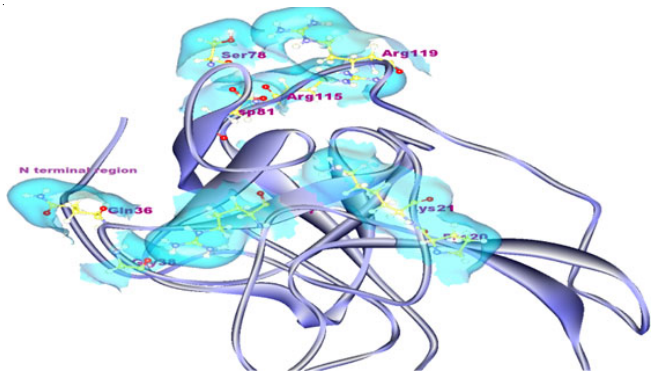

Fig. 8. Active site region of KLK-12 at the N terminal ranges are Pro20, Lys21, Gln36, Gly38, Ser78, Asp81, Arg115, Arg119 and Arg157, The hydrophobic regions are depicted in Cyan

The interactions present in the best KLK-12-CYR 61 as described in the literature have preserved Cys, His and Asp catalytic residues. The results of the CASTp and active site prediction server revealed that the region from amino acid Ile 22 to His 150 in the Tryp_SPc domain holds a large hydro-phobic pocket located in the C-terminal region of the KLK-12 protein.

Substantiating the findings of the PPI analysis and the results of active site prediction methods, it is inferred that the KLK-12 region from Ile 22 to His 150 serves as an active site area responsible for signaling angiogenesis. Virtual screening studies were performed using AUTODOCK tools 1.5.6 [37]. Ligand centered maps were generated by Auto Grid program with a spacing of 0.375 Å and grid dimensions of 44 × 58 × 44 Å^3. Grid box center was set to coordinate -27.285, -4.168 and -8.415 in *x*, *y* and *z*, respectively as shown in Fig. 9.

In the preserved domain region of KLK-12 protein, virtual screening was carried out, resulting in the top-rated ligand molecules with 9 different poses. The docking poses and ligand ranking is based on the empirical score feature of Vina approxi-

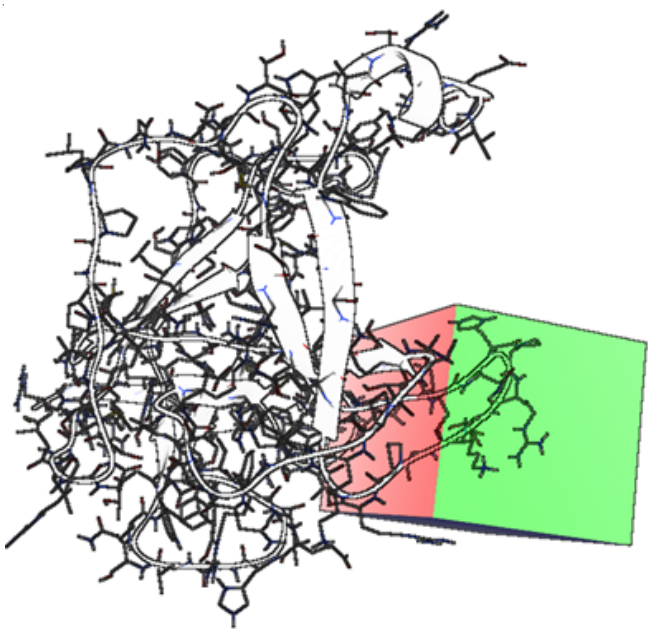

Fig. 9. Grid box for virtual screening of KLK-12 protein. KLK-12 protein represented as grey cartoon and grid box as square box in green and red

mating the binding affinity in kcal/mol. The software selects ligands with the best docking positions from the input. The virtual screening output consists of top-ranking docked complexes based on binding energies and physico-chemical properties. For a final collection of the best compound candidates, the 9 best-scored poses for each compound were retrieved and further ranked using the Accelrys Discovery Studio Visualizer 3.5 [52].

One of the most difficult aspects of virtual screening is analysis and filtering because the aim is to find a few potential leads from a wide body of docked outcomes. Filtering based on predicted docking energy, combined with the existence of key interactions in the system, acquires successful results. A detailed analysis of the results of the virtual screening reveals that the KLK-12 ligand complex interactions indicate the high affinity of ligands to proteins with sufficient binding energy (-9.9 to -10.2 Kcal/mol) and the pharmacokinetic properties of the top ten ligand molecules (L1 to L10) were prioritized based on the H-bond and pi-interactions (Table-5).

The hydrogen bond interactions with Accelrys Discovery Studio Visualizer 3.5 are visualized in Fig. 10 (L1-L10). The H bond interactions are significant (1.8103 to 2.49 Å) throughout docked complexes. Hydrogen bond interactions with the amino acids Trp35, Gln36, Gly38, Trp82, His107 of the conserved domain KLK-12 are seen with new ligand molecules. Table-5 displays a sample of 10 docked molecules, prioritized based on the binding energy.

In Auto Dock, based on the parameters, various scaffolds of ligand molecules were recognized. The ligand molecules are prioritized based on binding energies, RMSD, ligand interactions with a visual inspection. Ligands L1-L5, L7 and L10 have substituted carboxamide, L6 has substituted benzamide, L8 has substituted propanamide, L9 has substituted quinazoline amine derivatives and all derivatives have a higher binding affinity with a binding energy of -9.9 to -10.2 kcal/mol.

Ligands L1 and L5 are derivatives of carboxamide quinoline, L2 a derivative of carboxamide pyrimidine, L3 a derivative of carboxamide isochromene, L7 a derivative of indole-2-carboxamide and L10 a derivative of carboxamide pyridine. Ligands L1 to L4, L9 and L10 were found to possess a common trifluoromethyl phenyl group as a substituent. Gln36 and Gly38 residues were found to interact with the natural substrate, which confirms their biological activity in the protein KLK-12. Table-5 displays the arrangement of the ligand molecules with their energy values, hydrogen bond and pi-bond distances. Several scientists [53-56] have also used similar protocols to discover new scaffolds for selective protein targets. The study identified pharmacophores that bind to KLK-12 proteins with carboxamide and benzamide substitution ligands such as quinoline and pyrimidine derivatives with the highest affinity (10.2 kcal/mol). Among the 10 new scaffolds with stronger hydrogen bond interaction, L3, L4 and L7 molecules function as potent antiangiogenic ligands against KLK-12 protein and acted as pathological angiogenesis antagonists in cancer.

The ligand molecules from virtual screening studies show a stronger affinity with good docking interactions and binding

TABLE-5
LIGANDS AND THEIR INTERACTIONS AT ACTIVE SITE OF KLK-12 OBTAINED FROM VIRTUAL SCREENING

S. No.	Ligand IUPAC name	Hydrogen bond interactions and bond length (BL in Å)	Energy (kcal/mol)
L1	2-Amino-*N*-[1-(naphthalen-1-yl)ethyl]-7-(trifluoromethyl)quinoline-3-carboxamide	H17::Gln36(O) 2.2884)	-10.2
L2	5-(1,3-Benzodioxol-5-yl)-*N*-(3,5-dimethylphenyl)-7-(trifluoromethyl)pyrazolo[1,5-*a*]-pyrimidine-2-carboxamide	H10::Gln36 (O) 2.4409) O3::Trp82 (O) (2.2535)	-10.2
L3	1-Oxo-4-phenyl-N-[3-(trifluoromethyl)phenyl]-1*H*-isochromene-3-carboxamide	H1::Gln36 (H)1.9167) O1::Gly38 (H) (2.1204)	-10.1
L4	9-Methyl-*N*-[3-(trifluoromethyl)phenyl]tetracyclo[6,6,2,$O^{2,7}$,$O^{11,12}$]hexadeca-2,4,6,11,13,15-hexene-9-carboxamide	H16::Gln36 (O) (1.8103)	-10.1
L5	2-Phenyl *N*-[4-(2-methoxy phenyl)-4,5-dihydro-1,3 thiazol-2-yl]quinoline-4-carboxamide	H9::Gln36 (O) (2.4341)	-10.1
L6	4-Chloro-*N*-[(6-phenylpyrrolo[2,1-*a*]phthalazin-3-yl)methyl]benzamide	O1::Trp82 (H) (2.4989)	-10
L7	*N*-(4-Methylbenzyl)-3-[(4-methylphenyl)sulfanyl]-1*H*-indole-2-carboxamide	H18::Trp35 (O) (1.9698) H8::Gln36 (O) (1.9733)	-10
L8	*N*-(7,7-Dimethyl-5-oxo-5,6,7,8-tetrahydroquinazolin-2-yl)-2-(1,3-dioxo-1,3-dihydro-2*H*-isoindol-2-yl)propanamide	O3::His107 (O)(2.0350)	-10
L9	*N*-[(4-Pyrimidin-yl)benzyl]-2-[(2-(trifluoromethyl)phenyl]quinazolin-4 amine	F1::Trp82 (H) (2.1881) H10:Trp35 (O) (2.4238) H10:Gln36 (O)(2.3450)	-9.9
L10	*N*-Phenyl-4-[4-(trifluoromethyl)phenyl]-6,7-dihydrothieno[3,2-*c*]pyridine-5(4*H*)-carboxamide	H12::Gln36 (O) (2.4315)	-9.9

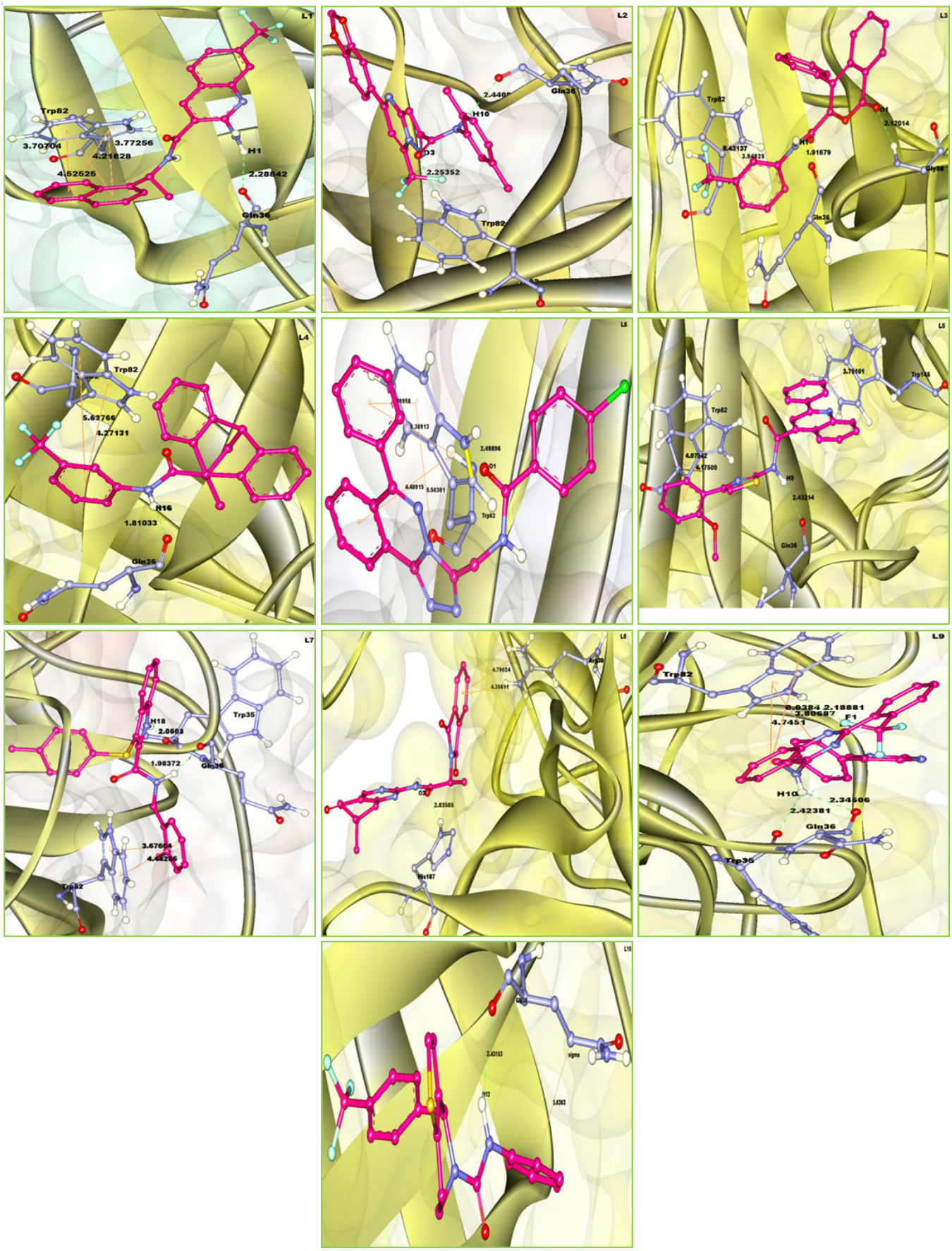

Fig. 10. Ligand interactions of KLK-12 obtained from virtual screening. 3D structure of the KLK-12 protein is represented in orange solid ribbon with interacting residues in stick model (Green) and the ligand molecule in ball and stick model (Pink). Intermolecular hydrogen bonds are shown in green dotted lines. Amino acids represented as three letter codes

energies. The newly discovered ligand molecules can be considered for further development of new leads against pathological angiogenesis and cancer. ADMET evaluation is a crucial stage of the drug development process before a pre-clinical trial. The ADME is evaluated based on physico-chemical properties for the established L1-L10 ligands that show affinity to KLK-12. Table-6 shows all ligand molecules having a permissible and acceptable pharmacokinetic spectrum of values, such as MW < 500 Daltons, HBA < 10, HBD < 5, log P < 5.6, TPSA < 120 Å.

To optimize the pharmacokinetic and pharmaceutical properties, the newly identified ligands show strong scores for Lipinski's rule of five and Jorgensen's rule of three, octanol/water partition coefficient, molecular weight (MW), hydrogen bond acceptor (HBA), hydrogen bond donor (HBD), solubility (log P), topological polar surface area (TPSA).

The Lipinski rule of 5 and Jorgensen's rule of 3 are followed by the 10 ligands, suggesting strong absorption and bioavailability. In contrast to other ligands, ligands L4 and L7 show stronger hydrogen bonds to the amino acid residues of KLK-12. The interactions with the amino acid residues of 10 ligands are visualized in Fig. 10.

Fig. 11 is a predictive model, the BOILED-Egg for the gastrointestinal and BBB prediction. The model plot is based on TPSA *vs.* log p, shows the white region is the physico-chemical space of molecules with highest probability of being absorbed by the gastrointestinal tract and the yellowregion (yolk) is the physico-chemical space of molecules with highest probability to permeate to the brain. Among the 10 ligands, L4 and L9 were out of the bioavailability zones [57], whereas L6 and L7 crossed the BBB hence are not suitable for the non-CNS category drugs. While rest of the ligands *viz.* L1, L2, L3, L5, L8, L10 are hydrophilic and suitable for oral inhibitor category of the drugs. Substrates of P-glycoprotein (PGA) are susceptible to changes in pharmacokinetics due to drug interactions with P-gp inhibitors or inducers PGA over expression is one of the main mechanisms behind decreased intracellular drug accumulation in various cancers [58]. Except for L3 ligand, other ligands (L1, L2, L3, L5, L8, L10) are PGA +, indicating the ligands are PGA inducing drug like mole-cules. The mentioned ADME properties include the Jorgensen Lipinski law (as most anti-cancer agents demonstrate cardiovascular toxicity) [59]. The pharmacokinetic properties included in the study, demonstrate the quality of new chemical structures are allowable ADME properties and lower toxicity of the various scaffolds.

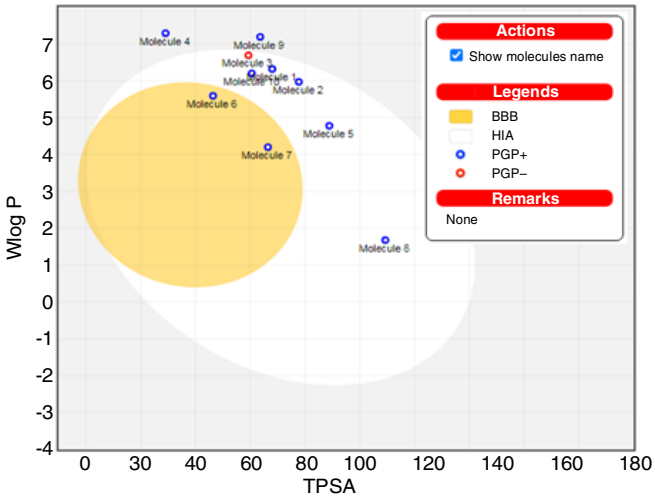

Fig. 11. BOILED-Egg predictive model

ADMET assessment before a pre-clinical trial is a critical stage of the drug development process. The ADME is evaluated based on physico-chemical properties for the established L1-L10 ligands that show affinity to KLK-12. Lipophilicity (log p) is a measure of efficient drug transport and high lipophilicity (0.09 to 5.5) and the ability to pass passively through the transcellular route are present in all ligands in this study. Inadequate levels of a drug that passes through the blood-brain barrier (BBB) can lead to central nervous system (CNS) adverse effects [60]. For the determination of the BBB values, the polar surface area is a critical parameter. Polar surface area values are within an acceptable range for all known ligands, *i.e.* ~ 120 (Å) and have strong overall ADME properties. As a result, the drug-like properties reported from virtual screening have been improved by L6 and L7 ligands, have synthetic viability compared to existing drugs and can therefore be considered for the design of new KLK-12 protein inhibitors and serve as a candidate drug for cancer pathogenic angiogenesis.

Conclusion

The 3D structure of KLK-12 protein, generated is a good quality model and comparable to the NMR resolved protein structures. Protein-protein docking of KLK-12 with CYR61 gave an insight into the residues of binding at the active site of KLK-12 protein. Virtual screening results identified the new ligand molecules with a permissible range of pharmacokinetic properties, have functional groups carboxamide, isoindole and quinazoline amines as common pharmacophore moieties. The

TABLE-6
PREDICTED ADME PROPERTIES OF THE DOCKED MOLECULES

Ligand No.	Energy	Is lead like	HBA	HBD	log P	MW	TPSA
L1	-10.2	Y	4	3	5.70	409.404	68.74
L2	-10.2	Y	7	1	4.62	454.401	77.75
L3	-10.1	Y	4	1	5.02	409.357	59.31
L4	-10.1	Y	2	1	5.64	407.428	29.10
L5	-10.1	Y	5	1	5.68	437.513	92.35
L6	-10	Y	6	1	4.09	413.859	72.18
L7	-10	Y	3	2	5.95	386.509	70.19
L8	-10	Y	8	1	1.79	392.408	109.33
L9	-9.9	Y	5	1	5.80	457.450	63.59
L10	-9.9	Y	3	1	4.93	402.433	60.58

The permissible ADME values are as follows: MW < 500, HBD < 5, HBA <10, log P < 5.6, TPSA ≤ 120 Å.

new lead molecules (L1 to L10) were prioritized based on the binding energy and physio-chemical properties. Ligands identified in the virtual screening studies are derivatives of substituted carboxamide (L1, L5, L2, L3, L7, L10) or pthalazin methyl benzamide (L6) or isoindole propanamide derivative (L8) or quinazoline amine derivative (L9). The amino acid residues Trp35, Gln36, Gly38, Trp82, His107 of KLK-12 protein have putative binding interactions with these ligand molecules. Among 10 new scaffolds, L3 (isochromene carboxamide) have stronger hydrogen bond interaction behave as potent antiangiogenic ligands by inhibiting the protein KLK-12 and acted as antagonists for pathological angiogenesis in cancer.

ACKNOWLEDGEMENTS

The authors are thankful to The Principal and The Head, Department of Chemistry, University College of Science, Saifabad, Osmania University, Hyderabad, India for providing the research facilities to carry out this work.

REFERENCES

1. D. Hanahan and R.A. Weinberg, Hallmarks of Cancer: The Next Generation, *Cell*, **144**, 646 (2011); https://doi.org/10.1016/j.cell.2011.02.013
2. L.A. Liotta and E.C. Kohn, The Microenvironment of the Tumour-Host Interface, *Nature*, **411**, 375 (2001); https://doi.org/10.1038/35077241
3. J.A. Aguirre-Ghiso, Models, Mechanisms and Clinical Evidence for Cancer Dormancy, *Nat. Rev. Cancer*, **7**, 834 (2007); https://doi.org/10.1038/nrc2256
4. Z. Ahmed and R. Bicknell, Angiogenic Signalling Pathways, *Mol. Biol.*, **467**, 3 (2009); https://doi.org/10.1007/978-1-59745-241-0_1
5. P. Carmeliet, Angiogenesis in Life, Disease and Medicine, *Nature*, **438**, 932 (2005); https://doi.org/10.1038/nature04478
6. C.A. Borgoño, I.P. Michael and E.P. Diamandis, Human Tissue Kallikreins: Physiologic Roles and Applications in Cancer, *Mol. Cancer Res.*, **2**, 257 (2004).
7. E.P. Diamandis, G.M. Yousef, J. Clements, L.K. Ashworth, S. Yoshida, T. Egelrud, P.S. Nelson, S. Shiosaka, S. Little, H. Lilja, U.H. Stenman, H.G. Rittenhouse and H. Wain, New Nomenclature for the Human Tissue Kallikrein Gene Family, *Clin. Chem.*, **46**, 1855 (2000); https://doi.org/10.1093/clinchem/46.11.1855
8. V.L. Koumandou and A. Scorilas, Evolution of the Plasma and Tissue Kallikreins, and their Alternative Splicing Isoforms, *PLoS One*, **8**, 68074 (2013); https://doi.org/10.1371/journal.pone.0068074
9. H. Lilja, A Kallikrein-like Serine Protease in Prostatic Fluid Cleaves the Predominant Seminal Vesicle Protein, *J. Clin. Invest.*, **76**, 1899 (1985); https://doi.org/10.1172/JCI112185
10. M.M. Webber, A. Waghray and D. Bello, Prostate-Specific Antigen, A Serine Protease, Facilitates Human Prostate Cancer Cell Invasion, *Clin. Cancer Res.*, **1**, 1089 (1995).
11. G.M. Yousef, A. Magklara and E.P. Diamandis, KLK12 Is a Novel Serine Protease and a New Member of the Human Kallikrein Gene Family—Differential Expression in Breast Cancer, *Genomics*, **69**, 331 (2000); https://doi.org/10.1006/geno.2000.6346
12. A. Guillon-Munos, K. Oikonomopoulou, N. Michel, C.R. Smith, A. Petit-Courty, S. Canepa, P. Reverdiau, N. Heuzè-Vourc'h, E.P. Diamandis and Y. Courty, Kallikrein-Related Peptidase 12 Hydrolyzes Matricellular Proteins of the CCN Family and Modifies Interactions of CCN1 and CCN5 with Growth Factors, *J. Biol. Chem.*, **286**, 25505 (2011); https://doi.org/10.1074/jbc.M110.213231
13. J.A. Clements, N.M. Willemsen, S.A. Myers and Y. Dong, The Tissue Kallikrein Family of Serine Proteases: Functional Roles in Human Disease and Potential as Clinical Biomarkers, *Crit. Rev. Clin. Lab. Sci.*, **41**, 265 (2004); https://doi.org/10.1080/10408360490471931
14. X.S. Puente, L.M. Sánchez, C.M. Overall and C. López-Otín, Human and Mouse Proteases: A Comparative Genomic Approach, *Nat. Rev. Genet.*, **4**, 544 (2003); https://doi.org/10.1038/nrg1111
15. J.C. Davis, L. Furstenthal, A.A. Desai, T. Norris, S. Sutaria, E. Fleming and P. Ma, The Microeconomics of Personalized Medicine: Today's Challenge and Tomorrow's Promise, *Nat. Rev. Drug Discov.*, **8**, 279 (2009); https://doi.org/10.1038/nrd2825
16. S. Jakka and M. Rossbach, An Economic Perspective on Personalized Medicine, *HUGO J.*, **7**, 1 (2013); https://doi.org/10.1186/1877-6566-7-1
17. D.E. Pritchard, F. Moeckel, M.S. Villa, L.T. Housman, C.A. McCarty and H.L. McLeod, Strategies for Integrating Personalized Medicine into Healthcare Practice, *Per. Med.*, **14**, 141 (2017); https://doi.org/10.2217/pme-2016-0064
18. E. Yuriev, J. Holien and P.A. Ramsland, Improvements, Trends, and New Ideas in Molecular Docking: 2012–2013 In Review, *J. Mol. Recognit.*, **28**, 581 (2015); https://doi.org/10.1002/jmr.2471
19. V. Malkhed, K.K. Mustyala, S.R. Potlapally and U. Vuruputuri, Identification of Novel Leads Applying *in silico* Studies for Mycobacterium Multidrug Resistant (Mmr) Protein, *J. Biomol. Struct. Dyn.*, **32**, 1889 (2014); https://doi.org/10.1080/07391102.2013.842185
20. R. Dumpati, V. Ramatenki, R. Vadija, S. Vellanki and U. Vuruputuri, Structural Insights into Suppressor of Cytokine Signaling 1 Protein-Identification of New Leads for Type 2 *Diabetes mellitus*, *J. Mol. Recognit.*, **31**, e2706 (2018); https://doi.org/10.1002/jmr.2706
21. C.M. Labbé, J. Rey, D. Lagorce, M. Vavruša, J. Becot, O. Sperandio, B.O. Villoutreix, P. Tufféry and M.A. Miteva, MTiOpenScreen: A Web Server for Structure-based Virtual Screening, *Nucleic Acids Res.*, **43**, W448 (2015); https://doi.org/10.1093/nar/gkv306
22. K.K. Mustyala, V. Malkhed, V.R.R. Chittireddy and U. Vuruputuri, Identification of Small Molecular Inhibitors for Efflux Protein: DrrA of *Mycobacterium tuberculosis*, *Cell. Mol. Bioeng.*, **9**, 190 (2016); https://doi.org/10.1007/s12195-015-0427-2
23. B. Boeckmann, A. Bairoch, R. Apweiler, M.-C. Blatter, A. Estreicher, E. Gasteiger, M.J. Martin, K. Michoud, C. O'Donovan, I. Phan, S. Pilbout and M. Schneider, The SWISS-PROT Protein Knowledge Base and its Supplement TrEMBL in 2003, *Nucleic Acids Res.*, **31**, 365 (2003); https://doi.org/10.1093/nar/gkg095
24. The UniProt Consortium, UniProt: A Hub for Protein Information, *Nucleic Acids Res.*, **43**, D204 (2015); https://doi.org/10.1093/nar/gku989
25. P. Artimo, M. Jonnalagedda, K. Arnold, D. Baratin, G. Csardi, E. de Castro, S. Duvaud, V. Flegel, A. Fortier, E. Gasteiger, A. Grosdidier, C. Hernandez, V. Ioannidis, D. Kuznetsov, R. Liechti, S. Moretti, K. Mostaguir, N. Redaschi, G. Rossier, I. Xenarios and H. Stockinger, ExPASy: SIB Bioinformatics Resource Portal, *Nucleic Acids Res.*, **40**, W597 (2012); https://doi.org/10.1093/nar/gks400
26. E. Gasteiger, ExPASy: the Proteomics Server for In-Depth Protein Knowledge and Analysis, *Nucleic Acids Res.*, **31**, 3784 (2003); https://doi.org/10.1093/nar/gkg563
27. A. Pertsemlidis and J.W. Fondon III, Having a BLAST with Bioinformatics (and Avoiding BLASTphemy), *Genome Biol.*, **2**, 1 (2001); https://doi.org/10.1186/gb-2001-2-10-reviews2002
28. J.A. Cuff and G.J. Barton, Evaluation and Improvement of Multiple Sequence Methods for Protein Secondary Structure Prediction, *Proteins*, **34**, 508 (1999); https://doi.org/10.1002/(SICI)1097-0134(19990301)34:4<508::AID-PROT10>3.0.CO;2-4
29. J. Soding, A. Biegert and A.N. Lupas, The HHpred Interactive Server for Protein Homology Detection and Structure Prediction, *Nucleic Acids Res.*, **33**, W244 (2005); https://doi.org/10.1093/nar/gki408

30. K. Bhargavi, P.K. Chaitanya, D. Ramasree, M. Vasavi, D.K. Murthy and V. Uma, Homology Modeling and Docking Studies of Human Bcl-2L10 Protein, *J. Biomol. Struct. Dyn.*, **28**, 379 (2010); https://doi.org/10.1080/07391102.2010.10507367
31. V. Ahola, T. Aittokallio, M. Vihinen and E. Uusipaikka, A Statistical Score for Assessing the Quality of Multiple Sequence Alignments, A Statistical Score for Assessing the Quality of Multiple Sequence Alignments, *BMC Bioinformatics*, **7**, 484 (2006); https://doi.org/10.1186/1471-2105-7-484
32. A. Šali, L. Potterton, F. Yuan, H. van Vlijmen and M. Karplus, Evaluation of Comparative Protein Modeling by MODELLER, *Proteins*, **23**, 318 (1995); https://doi.org/10.1002/prot.340230306
33. N. Guex and M.C. Peitsch, SWISS-MODEL and the Swiss-Pdb Viewer: An Environment for Comparative Protein Modeling, *Electrophoresis*, **18**, 2714 (1997); https://doi.org/10.1002/elps.1150181505
34. R.A. Laskowski, M.W. Macarthur, D.S. Moss and J.M. Thornton, PROCHECK: A Program to Check the Stereochemical Quality of Protein Structures, *J. Appl. Cryst.*, **26**, 283 (1993); https://doi.org/10.1107/S0021889892009944
35. M. Wiederstein and M.J. Sippl, ProSA-Web: Interactive Web Service for the Recognition of Errors in Three-dimensional Structures of Proteins, *Nucleic Acids Res.*, **35**, W407 (2007); https://doi.org/10.1093/nar/gkm290
36. J. Dundas, Z. Ouyang, J. Tseng, A. Binkowski, Y. Turpaz and J. Liang, CASTp: Computed Atlas of Surface Topography of Proteins with Structural and Topographical Mapping of Functionally Annotated Residues, *Nucleic Acids Res.*, **34**, W116 (2006); https://doi.org/10.1093/nar/gkl282
37. D. Duhovny, R. Nussinov and H.J. Wolfson, Efficient Unbound Docking of Rigid Molecules, In: Lect. Notes Comput. Sci. (Including Subser. Lect. Notes Artif. Intell. Lect. Notes Bioinformatics) (2002).
38. D. Schneidman-Duhovny, Y. Inbar, R. Nussinov and H.J. Wolfson, PatchDock and SymmDock: Servers for Rigid and Symmetric Docking, *Nucleic Acids Res.*, **33**, W363 (2005); https://doi.org/10.1093/nar/gki481
39. D.S. Goodsell and A.J. Olson, Automated Docking of Substrates to Proteins by Simulated Annealing, *Proteins Struct. Funct. Bioinform.*, **8**, 195 (1990); https://doi.org/10.1002/prot.340080302
40. G.M. Morris, R. Huey, W. Lindstrom, M.F. Sanner, R.K. Belew, D.S. Goodsell and A.J. Olson, AutoDock4 and AutoDockTools4: Automated Docking with Selective Receptor Flexibility, *J. Comput. Chem.*, **30**, 2785 (2009); https://doi.org/10.1002/jcc.21256
41. M.M. Jaghoori, B. Bleijlevens and S.D. Olabarriaga, 1001 Ways to Run AutoDock Vina for Virtual Screening, *J. Comput. Aided Mol. Des.*, **30**, 237 (2016); https://doi.org/10.1007/s10822-016-9900-9
42. M.A. Rauf, S. Zubair and A. Azhar, Ligand Docking and Binding Site Analysis with Pymol and Autodock/Vina, *Int. J. Basic Appl. Sci.*, **4**, 168 (2015); https://doi.org/10.14419/ijbas.v4i2.4123
43. Y. Wang, T. Suzek, J. Zhang, J. Wang, S. He, T. Cheng, B.A. Shoemaker, A. Gindulyte and S.H. Bryant, PubChem BioAssay: 2014 Update, *Nucleic Acids Res.*, **42**, D1075 (2014); https://doi.org/10.1093/nar/gkt978
44. A. Daina, O. Michielin and V. Zoete, SwissADME: A Free Web Tool to Evaluate Pharmacokinetics, Drug-likeness and Medicinal Chemistry Friendliness of Small Molecules, *Sci. Rep.*, **7**, 42717 (2017); https://doi.org/10.1038/srep42717
45. A. Daina and V. Zoete, A BOILED-Egg To Predict Gastrointestinal Absorption and Brain Penetration of Small Molecules, *ChemMedChem*, **11**, 1117 (2016); https://doi.org/10.1002/cmdc.201600182
46. M. Johnson, I. Zaretskaya, Y. Raytselis, Y. Merezhuk, S. McGinnis and T.L. Madden, NCBI BLAST: A Better Web Interface, *Nucleic Acids Res.*, **36**, 5 (2008); https://doi.org/10.1093/nar/gkn201
47. S. Karlin and S.F. Altschul, Methods for Assessing the Statistical Significance of Molecular Sequence Features by Using General Scoring Schemes, *Proc. Natl. Acad. Sci. USA*, **87**, 2264 (1990); https://doi.org/10.1073/pnas.87.6.2264
48. A. Drozdetskiy, C. Cole, J. Procter and G.J. Barton, JPred4: A Protein Secondary Structure Prediction Server, *Nucleic Acids Res.*, **43**, 389 (2015); https://doi.org/10.1093/nar/gkv332
49. J. Söding, Protein Homology Detection by HMM-HMM Comparison, *Bioinformatics*, **21**, 951 (2005); https://doi.org/10.1093/bioinformatics/bti125
50. W. Kaplan and T.G. Littlejohn, Swiss-PDB Viewer (Deep View), *Brief. Bioinform.*, **2**, 195 (2001); https://doi.org/10.1093/bib/2.2.195
51. M. Feig, Local Protein Structure Refinement *via* Molecular Dynamics Simulations with locPREFMD, *J. Chem. Inf. Model.*, **56**, 1304 (2016); https://doi.org/10.1021/acs.jcim.6b00222
52. D. Schneidman-Duhovny, Y. Inbar, V. Polak, M. Shatsky, I. Halperin, H. Benyamini, A. Barzilai, O. Dror, N. Haspel, R. Nussinov and H.J. Wolfson, Taking Geometry to its Edge: Fast Unbound Rigid (And Hinge-bent) Docking, *Proteins*, **52**, 107 (2003); https://doi.org/10.1002/prot.10397
53. R. Vadija, K.K. Mustyala, N. Nambigari, R. Dulapalli, R.K. Dumpati, V. Ramatenki, S.P. Vellanki and U. Vuruputuri, Homology Modeling and Virtual Screening Studies of FGF-7 Protein-A Structure-based Approach to Design New Molecules Against Tumor Angiogenesis, *J. Chem. Biol.*, **9**, 69 (2016); https://doi.org/10.1007/s12154-016-0152-x
54. S.P. Vellanki, R. Dulapalli, B. Kondagari, N. Nambigari, R. Vadija, V. Ramatenki, R.K. Dumpati and U. Vuruputuri, Structural Evaluation and Binding Mode Analysis of CCL19 and CCR7 Proteins-Identification of Novel Leads for Rheumatic and Autoimmune Diseases: An *In silico* study, *Interdiscip. Sci. Comput. Life Sci.*, **10**, 346 (2018); https://doi.org/10.1007/s12539-017-0212-0
55. N.M.F.S.A. Cerqueira, D. Gesto, E.F. Oliveira, D. Santos-Martins, N.F. Brás, S.F. Sousa, P.A. Fernandes and M.J. Ramos, Receptor-based Virtual Screening Protocol for Drug Discovery, *Arch. Biochem. Biophys.*, **582**, 56 (2015); https://doi.org/10.1016/j.abb.2015.05.011
56. M.W. Chang, C. Ayeni, S. Breuer and B.E. Torbett, Virtual Screening for HIV Protease Inhibitors: A Comparison of AutoDock 4 and Vina, *PLoS One*, **5**, e11955 (2010); https://doi.org/10.1371/journal.pone.0011955
57. S. Tian, J. Wang, Y. Li, D. Li, L. Xu and T. Hou, The Application of *in silico* Drug-Likeness Predictions in Pharmaceutical Research, *Adv. Drug Deliv. Rev.*, **86**, 2 (2015); https://doi.org/10.1016/j.addr.2015.01.009
58. A. Breier, L. Gibalova, M. Seres, M. Barancik and Z. Sulova, New Insight into P-Glycoprotein as a Drug Target, *Anticancer. Agents Med. Chem.*, **13**, 159 (2012); https://doi.org/10.2174/1871520611307010159
59. S.J. Park, H. Baars, S. Mersmann, H. Buschmann, J.M. Baron, P.M. Amann, K. Czaja, H. Hollert, K. Bluhm, R. Redelstein and C. Bolm, *N*-Cyano Sulfoximines: COX Inhibition, Anticancer Activity, Cellular Toxicity, and Mutagenicity, *ChemMedChem*, **8**, 217 (2013); https://doi.org/10.1002/cmdc.201200403
60. C. Betsholtz, Double Function at the Blood-Brain Barrier, *Nature*, **509**, 432 (2014); https://doi.org/10.1038/nature13339